

Article

Modelling of Ozone Mass-Transfer through Non-Porous Membranes for Water Treatment

Matthew J. Berry¹, Caitlin M. Taylor^{1,2,3}, William King¹, Y. M. John Chew^{1,2,3,*} and Jannis Wenk^{1,2,3,*}

¹ Department of Chemical Engineering, University of Bath, Claverton Down, Bath BA2 7AY, UK; mb846@bath.ac.uk (M.J.B.); c.taylor2@bath.ac.uk (C.M.T.); wk241@bath.ac.uk (W.K.)

² Centre for Sustainable Chemical Technologies, University of Bath, Claverton Down, Bath BA2 7AY, UK

³ Water Innovation & Research Centre, University of Bath, Claverton Down, Bath BA2 7AY, UK

* Correspondence: y.m.chew@bath.ac.uk (Y.M.J.C.); j.h.wenk@bath.ac.uk (J.W.);

Tel.: +44-1225-38-6132 (Y.M.J.C.); +44-1225-38-3246 (J.W.)

Received: 20 May 2017; Accepted: 19 June 2017; Published: 23 June 2017

Abstract: The mass transfer of ozone and oxygen into water through non-porous membranes was studied using computational fluid dynamics (CFD) modelling and fundamental convection-diffusion theory. Ozone is a gaseous oxidant that is widely applied in drinking water treatment. Membrane contactors are an alternative to conventional gas dispersion methods for injection of ozone gas mixtures into water. Few studies have explored computational approaches for membrane based ozone transport. In this investigation, quantitative concentration profiles across a single polydimethylsiloxane (PDMS) capillary membrane tube with internal gas flow and external liquid flow were obtained, including single mass transfer resistances and overall mass transfer coefficients for ozone and oxygen for varying membrane lengths, thicknesses, and laminar flow liquid side velocities. Both the influence of diffusivity and solubility of gases in the membrane were considered with the applied model. Previous studies have neglected the solubility of gases in the membranes in their analysis of ozone and oxygen gas fluxes. This work shows that the solubility has a significant impact of the overall mass transfer coefficients, in particular for oxygen. The main resistance for ozone was found in the liquid side, while for oxygen it was in the membrane. Mass transfer correlations based on heat transfer analogies revealed Sherwood (Sh) correlations for ozone and oxygen with good agreement to literature data, indicating that the applied computational model returns sensible results. The outcome of this study provides an initial basis for computational predictions of ozone and oxygen mass transfer for different membrane materials, flow conditions and reactor designs.

Keywords: water treatment; ozone; oxygen; non-porous membranes; solubility; mass transfer coefficient; concentration; diffusion; gas separation; computational fluid dynamics (CFD); film theory

1. Introduction

Ozone (O₃) is an oxidant and disinfectant that is being increasingly used for drinking water and waste water treatment [1]. Ozone gas has limited stability and needs to be produced on-site before being dissolved in water. The production of O₃ is an energy intensive process demanding ~10 to 20 kWh/kg O₃, when produced from oxygen (O₂) or air respectively [2]. The supply of pure O₂ is also an important cost factor. Traditionally, O₃ is dispersed by bubbling a gas mixture of typically 6% to 13% (wt) O₃ [2] into the water via bubble diffusers, injectors, or static mixers [3]. While the principles of direct gas-liquid mass transfer of O₃ into the aqueous phase are well understood [4–6], bubbling methods bear a number of disadvantages, such as locally inaccurate O₃ dosages due to short-circuiting [7,8], foam formation in treatment reactors [9], and uneconomic off-gas recovery. The off-gas contains mostly O₂ and residual amounts of O₃. In some treatment plants, the O₂ contained

in the off-gas is reused after residual O_3 destruction for the aeration of biological water treatment steps [10].

Membrane ozone contactors are an alternative to traditional dispersion methods. Gas transfer via membranes, including separation and purification of gases is an established industrial process [11]. The main advantage of membrane contactors is their well-defined, tailored membrane structure and the large contact surface area per volume in the reactor design. Further advantages of membrane contactors include predictable flow pathways on both the gas and the liquid side, including avoidance of the flow phenomena problems that dispersive processes face, easy scale-up by modular design, and straightforward recycling of the effluent gas stream because the gas does not take up impurities, such as moisture, during the process [2,12]. For ozonation processes, these advantages may result in economic recycling of unused oxygen and an overall increase in mass-transfer efficiency, which could eventually improve the energy efficiency of ozonation water treatment processes. Membrane contactors can be incorporated with standardised reactors with small footprint tubular designs and small cross sections for high linear flow rates [13]. Membranes, however, create an additional mass transfer resistance, which may significantly reduce the process efficiency. Material properties such as selectivity, permeability, mechanical strength, fouling affinity, and chemical reactivity (here mainly stability towards O_3), that affect longevity, need to be considered when calculating investment costs for membrane contactors [14,15].

Non-porous polymeric membranes are being successfully used in the process industry for separation of gas mixtures [16]. The potential for large-scale operation of O_3 is limited by membrane durability under extreme oxidizing conditions [17]. Therefore, the choice of the membrane material in O_3 applications is critical [18,19]. Chemical-resistant membranes that have been used for ozonation of water consist of ceramic materials [20–24] and fluorinated [13,25–29] or non-porous silicone based [26,30] polymers.

Several experimental studies have investigated the transport of O_3 from gas into liquid by using appropriate membrane contactor materials. A summary of these studies is shown in Table 1. Shanbhag and Sirkar, (1998) [31] explored the permeability and selectivity of oxygen, nitrogen, and ozone experimentally with a non-porous polydimethylsiloxane (PDMS) capillary membrane contacting system. They reported that the exposure to O_3 increases the general permeability of PDMS for gases and determined that O_3 permeability in PDMS is four times greater than that of O_2 . Pines et al. (2005) [13] reported the mass transfer rate of O_3 through porous polytetrafluoroethylene (PTFE) and polyvinylidene difluoride (PVDF) membranes and non-porous PTFE membranes using flat sheet contactor systems. Mass transfer coefficients and correlations, including the effect of the liquid side Reynold's number were explored. Phattaranawik et al. (2005) showed that ozone mass transfer via PVDF membranes with and without chemical reaction is controlled by the liquid film [32]. Stylianou et al. (2015) [22], investigated the mass transfer behaviour of O_3 in tubular porous ceramic membrane (Al_2O_3) contactors by looking at the effect of the liquid side Reynold's number on the overall mass transfer coefficient. Additionally, the ability of the contactor system to oxidise pesticides and an environmentally relevant fuel additive was examined.

Experimental studies generally provide a good indication on the ozone mass transfer in membrane contactor systems, however, using experimental approaches only, it can be challenging to generalise conclusions and to quantify and visualise gas concentration profiles and the individual mass transfer resistances across and along membrane sections, which is crucial, for example, to the dimension and optimisation of full-scale contactor systems. To address these challenges, in this study the performance of non-porous PDMS membranes for bubble-less transfer of ozone gas into the aqueous phase was investigated by using computational fluid dynamics (CFD) in combination with fundamental film theory. The computational work was conducted using COMSOL Multiphysics V5.2 to determine the concentration profiles of O_3 (and O_2) in the gas, membrane, and liquid phase, so that major mass transfer resistances could be identified. CFD has been widely used to explore flow phenomena and hydrodynamics in dispersive ozonation systems, to predict ozone mass transfer and improve

disinfection efficiency [33,34]. Most computational work on gas membrane contactors is related to carbon dioxide transport and separation [35–37], but limited studies are available on O_3 mass transfer through membranes specifically used in water treatment. For this study, PDMS membranes were chosen based on available literature data, because the material is readily commercially available and resistant to O_3 . The computational model developed in this study could be easily extended to include other membrane materials.

Table 1. Overview on ozone mass-transfer studies for different membrane contactor systems.

Membrane System	Gases Explored	Main Findings	Reference
PDMS, non-porous, capillary membrane contactor	O_2 , O_3 , N_2	Gas permeability, ozone permeability is four times greater than oxygen, PDMS solubility for gases increases after ozone exposure	[31]
PTFE, PVDF, porous and nonporous, flat sheet	O_3	Developed mass transfer coefficients and mass transfer correlations	[13]
Al_2O_3 ceramic, porous, tubular membrane contactor	O_3	Developed mass transfer coefficients	[22]
PVDF, porous, flat sheet	O_3 , O_2	Ozone mass transfer coefficient developed indirectly from oxygen transport	[32]

The goal of this study was to investigate the mass transport characteristics of O_3 and O_2 from a prescribed gas mixture, typically produced by state-of-the-art commercial ozone generators, to the bulk liquid phase through a non-porous membrane under flow conditions. Specifically, the objectives were (i) investigate the relationship between ozone mass transfer (e.g., concentration profiles and resistance distributions) and membrane properties; (ii) the effect of process conditions (e.g., length of membrane, thickness of membrane, liquid side velocity) on the mass transfer; and (iii) develop mathematical correlations to determine the overall mass transfer coefficient and compare them to the literature.

1.1. Theoretical Development

The transport of ozone-oxygen or ozone-air mixtures in non-porous polymeric membrane contactors is governed by the mass transfer in the gas and liquid films, the solubility laws, and the diffusivity of the ozone within the membrane material. Whitman's Film theory (1923) was the first attempt to model gas-liquid interfacial mass transfer [38]. Although the theory does not closely reproduce conditions in reality, it is commonly used to model gas-liquid mass transfer performance and then compare to experimental data. Figure 1 shows a conceptual model of mass transport of ozone from gas to liquid through a non-porous membrane. Ozone diffuses from the bulk gas phase, through a stagnant gas film, through the membrane, through a stagnant liquid film, and dissolves into the bulk liquid phase. The nomenclature, acronyms, and subscripts used for the theoretical development and throughout the article are listed in Abbreviations.

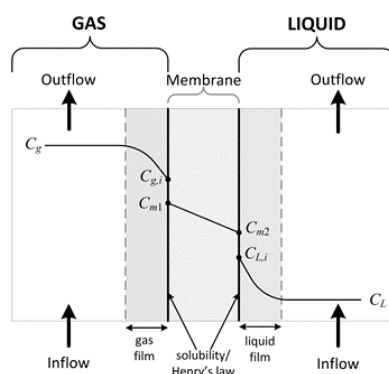


Figure 1. A schematic of a single tube membrane contactor under co-current flow conditions separating the gas and liquid phases, and the concentration profiles of O_3 in the different phases.

1.1.1. Gas Phase

The film theory assumes the presence of a laminar film where any turbulence in the bulk flow dissipates. In this film region, the concentration deviates from the bulk concentration moving to an interfacial concentration such that the molar flux can be expressed as:

$$N = k_g(C_g - C_{g,i}) \quad (1)$$

where N is the molar flux, k_g is the film side mass transfer coefficient, C_g is the concentration in the bulk and $C_{g,i}$ is the concentration at the gas–membrane interface on the gas side.

1.1.2. Membrane

The solubility of O_3 at the interface between the gas and non-porous polymeric membrane can be described in terms of a solution-diffusion mechanism where the gas permeability is determined by its diffusivity and solubility [26]:

$$\frac{C_{g,i}}{S} = C_{m1} \quad (2)$$

where C_{m1} is the concentration at the gas–membrane interface on the membrane side and S is the solubility constant of the gas in the membrane. Previous studies, e.g., [13,18] on O_3 mass transfer often assumed the concentration of O_3 at the gas–membrane is continuous i.e., $C_{g,i} = C_{m1}$. In this work, comparison of the concentration profile at the gas–membrane interface for both cases is presented.

The concentration at the interface between the membrane–liquid phases can be described by Henry's law [13]:

$$C_{L,i} = \frac{C_{m2}}{H} \quad (3)$$

where C_{m2} and $C_{L,i}$ are the concentrations at the membrane–liquid interface on the membrane and liquid side, respectively, and H is the Henry's Law constant.

Therefore, the mass transfer across the membrane can therefore be written as:

$$N = k_m(C_{m1} - C_{m2}) \quad (4)$$

where k_m is the mass transfer coefficient in the membrane.

1.1.3. Liquid Phase

The film theory is also assumed at the liquid phase side:

$$N = k_L(C_{L,i} - C_L) \quad (5)$$

where k_L is the mass transfer coefficient in the liquid film.

Combining Equations (1) to (5):

$$N = K_L \left(\frac{C_g}{S} - HC_L \right) \quad (6)$$

where the overall mass transfer coefficient, K_L , can be described by a series of resistance terms:

$$\frac{1}{K_L} = \frac{1}{Sk_g} + \frac{1}{k_m} + \frac{H}{k_L} \quad (7)$$

For a thin membrane i.e., typically when the membrane thickness to inner radius of membrane ratio is less than 0.2, the curvature effect is negligible such that the membrane surface can be

approximated to a flat plane. For some cases in this work the ratio is more than 0.2, thus the curvature of membrane needs to be taken into account such that Equation (7) becomes:

$$\frac{1}{K_L A_{outer}} = \frac{1}{S k_g A_{inner}} + \frac{1}{k_m A_m} + \frac{H}{k_L A_{outer}} \quad (8)$$

where A_{inner} , A_m , and A_{outer} are the area of the inner surface of the membrane, log mean area of the membrane and area of the outer surface of the membrane, respectively.

For steady state conditions, a mass balance on the ozone in the liquid phase can be expressed as:

$$\frac{dC_L}{dx} = \frac{1}{u_{L,mean}} K_L a \left(\frac{C_g}{S} - HC_L \right) \quad (9)$$

where $u_{L,mean}$ is the mean liquid velocity, a is the surface area of membrane per unit volume of liquid and x is the direction of flow. Integrating Equation (9) with the boundary conditions at $x = 0$, $C_L = 0$ (concentration of ozone at liquid inlet is zero) and at the liquid outlet, $x = L$, $C_L = C_{L,out}$ yields the following:

$$\frac{K_L a \cdot L}{u_{L,mean}} = \frac{1}{H} \ln \left\{ \frac{\frac{C_g}{S}}{\frac{C_g}{S} - HC_{L,out}} \right\} \quad (10)$$

2. Numerical Modelling

The CFD modelling package COMSOL Multiphysics 5.2 was used to simulate the mass transfer of ozone and oxygen through a capillary-sized non-porous PDMS membrane into water. Species and momentum conservation equations were coupled and solved to describe the transport of the gas mixture and liquid solvent simulating a co-current single hollow fibre membrane contactor. The set-up of the CFD model followed the steps outlined by Tu et al. (2012) [39]. A steady state condition was assumed in all mathematical models presented in this study.

2.1. Model Domain and Geometry

A 2-D axisymmetric domain (Figure 2) was used to model a single tube membrane contactor where ozone/oxygen gas mixtures flow in the tube and water flows parallel on the outside. The geometry was built based on the dimensions of the membrane tubes available from Dow Corning, i.e., Silastic® medical grade lab tubing. The three defined domains are the gas phase, the membrane, and the liquid phase. The dimensions of the geometry on tube, operating conditions, physical properties, and material data used in the simulation are summarised in Table 2.

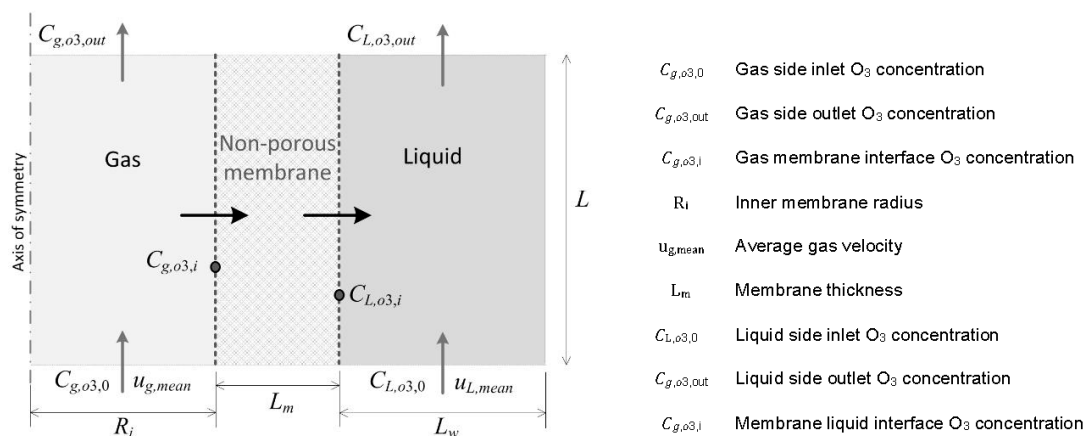


Figure 2. 2-D axisymmetric computational domain approximating the gas, membrane, and liquid phase, labelled with ozone concentrations and velocities.

Table 2. Numerical modelling parameters.

Parameter	Value (Range)	Unit	Reference
Inner membrane radius, R_i	0.51	mm	Manufacturer information ^a
Membrane thickness, L_m	0.57 (0.05–4.50)	mm	Manufacturer information ^a
Water layer thickness, L_W	4.42	mm	Estimated parameter ^b
Membrane length, L	500 (250–1250)	mm	Study parameter
O ₃ diffusivity in gas phase, $D_{g,o3}$	1.454×10^{-5}	$\text{m}^2 \text{s}^{-1}$	[40]
O ₃ diffusivity in water, $D_{L,o3}$	1.76×10^{-9}	$\text{m}^2 \text{s}^{-1}$	[2]
O ₃ diffusivity in the membrane, $D_{m,o3}$	2.96×10^{-9}	$\text{m}^2 \text{s}^{-1}$	Calculated via the PDMS-ozone permeability coefficient $Q_{m,o3}$ and the solubility coefficient of O ₃ in PDMS, S_{o3} ^c
O ₃ membrane permeability, $Q_{m,o3}$	1.05×10^{-12}	$\text{mol m}^{-1} \text{s}^{-1} \text{Pa}^{-1}$	[31]
O ₂ diffusivity in gas phase, $D_{g,o2}$	1.862×10^{-5}	$\text{m}^2 \text{s}^{-1}$	[41]
O ₂ diffusivity in water, $D_{L,o2}$	2.025×10^{-9}	$\text{m}^2 \text{s}^{-1}$	[2]
O ₂ diffusivity in membrane, $D_{m,o2}$	2.1×10^{-9}	$\text{m}^2 \text{s}^{-1}$	[31]
O ₃ inlet concentration in gas, $C_{g,o3,0}$	3.75 (0.41–6.25)	mol m^{-3}	Equates to 13% (wt) of ozone in ozonated oxygen under specified temperature and pressure conditions
O ₃ inlet concentration in water, $C_{L,o3,0}$	0	mol m^{-3}	Specified parameter
O ₂ inlet concentration in water, $C_{L,o2,0}$	0	mol m^{-3}	Specified parameter
Average gas velocity, $u_{g,mean}$	0.1	m s^{-1}	Experimental parameter
Average water velocity, $u_{L,mean}$	8×10^{-4} (4×10^{-4} –0.15)	m s^{-1}	The flow regime is assumed laminar in this work i.e., simulating the worst case scenario for mass transfer
Temperature, T	298.15	K	Isothermal condition was assumed throughout
Universal gas constant, R	8.314	$\text{J mol}^{-1} \text{K}^{-1}$	
Total pressure at gas inlet, p_{tot}	101325	Pa	Pressure at inlet is assumed to be atmospheric
Total gas concentration at inlet, C_{tot}	$p_{tot} / (RT)$	mol m^{-3}	
O ₂ inlet concentration in gas, $C_{g,o2,0}$	$C_{tot} - C_{g,o3,0}$ 37.12 (40.46–34.62)	mol m^{-3}	
O ₃ solubility in water, H_{o3}	$1 \times 10^{-4} RT_g$	-	[42]
O ₂ solubility in water, H_{o2}	$1.2 \times 10^{-5} RT_g$	-	[42]
O ₃ solubility in PDMS membrane, S_{o3}	0.881	-	[26]
O ₂ solubility in PDMS membrane, S_{o2}	0.201	-	[31]

Notes: ^a Silastic® Rx medical grade tubing from Dow Corning; ^b The value of water layer thickness is selected so that bulk concentration is not affected by this value; ^c The diffusivity $D_{m,o3}$ of ozone in the membrane is calculated by using the definition of the permeability coefficient $Q_{m,o3}$ for ozone through the PDMS polymer [31], $Q_{m,o3} = D_{m,o3} \times S_{i,o3}$, where $S_{i,o3}$ [$\text{mol m}^{-3} \text{Pa}^{-1}$] is the solubility value of ozone in PDMS reported in [26].

2.2. Meshing and Scaling

The computation domain was approximated using unstructured triangular elements (Figure 3a) and a mesh independence study (Figure 3b) was carried out. Denser mesh was set at the gas–membrane and membrane–liquid interfaces to improve accuracy. Figure 3b shows the concentrations of O₃ evaluated at the gas–membrane and membrane–liquid interfaces (see Figure 2) using varying numbers of elements. The Figure clearly suggests the values of the concentration are independent of the number of elements from 11,745, i.e., the ‘finer mesh’ setting in COMSOL. The optimal mesh choice based on accuracy and computing time, was, therefore, ‘finer mesh’ and was employed for all remaining simulations.

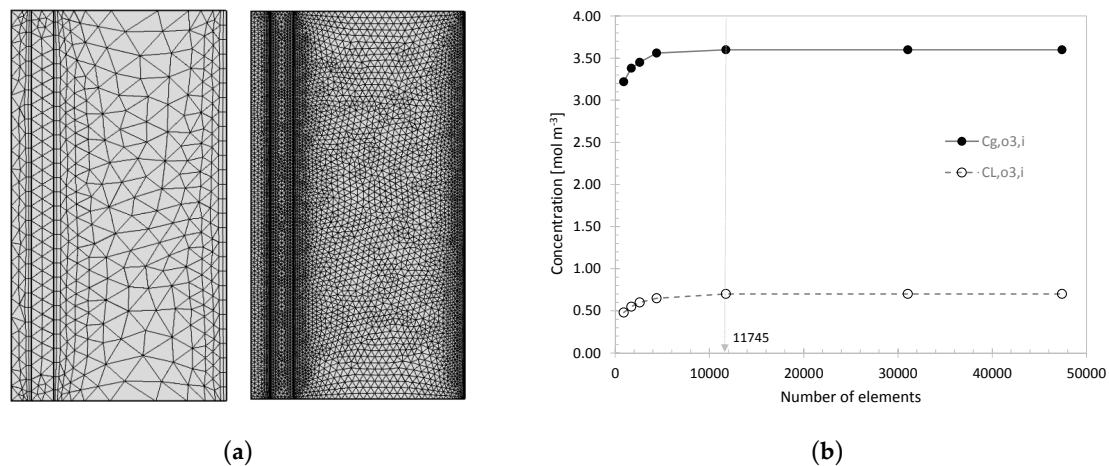


Figure 3. (a) Comparison of mesh distribution between ‘coarser—905 elements’ (left) and ‘finer—11,745 elements’ (right) mesh settings in COMSOL. The denser mesh was used at the fluid–membrane interfaces to ensure improved accuracy; (b) Example of the converged values of concentration of ozone at the gas–membrane (gas side, $C_{g,o3,i}$) and membrane–liquid interface (liquid side, $C_{L,o3,i}$) at 50% length of the membrane.

Scaling the model in the z -direction became necessary as the tube length being considered was much greater than the diameter and tube thickness which affected the meshing and therefore the numerical stability. A scaling factor of 50 was selected and applied to the tube length, diffusivities in the z -direction, and the gas and liquid velocities. The residual for successive iterations for all variables, i.e., the convergence criteria in all simulations, was set to 10^{-5} .

2.3. Governing Equations

The three computational domains considered were the gas section, the membrane section, and the liquid section. For each section, governing equations for momentum and species transport, including boundary conditions were specified:

$$1. \text{ Gas section } 0 \leq r \leq R_i$$

Momentum transport:

The gas mixture in the tube is assumed to be ideal and incompressible and the flow is treated as steady state, laminar, and Newtonian. It was also assumed that the operating pressure is 1 atmospheric so that it is reasonable to assume that gas is incompressible. The gravitational effect is also assumed to be negligible [41], hence the velocity can be described using the continuity and Navier–Stokes equations as follows:

$$\text{Continuity : } \nabla \cdot \mathbf{u}_g \quad (11)$$

$$\text{Navier–Stokes : } \rho_g (\mathbf{u}_g \cdot \nabla \mathbf{u}_g) = -\nabla p_g + \mu_g \nabla^2 \mathbf{u}_g \quad (12)$$

where \mathbf{u}_g is the velocity vector in the gas phase, and p_g is the pressure. The density and viscosity of the gas is assumed constant throughout as ρ_g and μ_g , respectively.

The boundary conditions were:

- i. Axial symmetry: no flow crossing the boundary, i.e., when $r = 0$, $u_{r,g} = 0$.
- ii. Membrane wall: no-slip, i.e., when $r = R_i$, $u_{z,g} = 0$.
- iii. The velocity in the r -directions at all the boundaries are almost zero, i.e., $u_{r,g} = 0$.

- iv. Tube inlet: flow is fully developed and velocity profile is parabolic, i.e., when $z = 0$,
 $u_{z,g} = 2u_{g,mean} \left[1 - \left(\frac{r}{R_i} \right)^2 \right]$ where $u_{g,mean}$ is the mean axial velocity in the gas phase.
- v. Tube outlet: flow is fully developed, i.e., when $z = L$, $\frac{\partial u_{z,g}}{\partial z} = 0$.

Species transport:

The steady state material balance for the transport of $j = O_2$ and O_3 in the gas phase is considered to be due to diffusion and convection and no reactions taking place. The species transport can be described as follows:

$$\mathbf{u}_g \cdot \nabla C_{g,j} = D_{g,j} \nabla^2 C_{g,j} \quad (13)$$

where $C_{g,j}$ is the concentration of j in the gas phase, $D_{g,j}$ is the mass diffusivity of j in the gas phase and is assumed to be isotropic. It is also assumed that there is no reaction taking place in the system.

The boundary conditions were:

- i. Axial symmetry: no material flow across the boundary, i.e., when $r = 0$, $\frac{\partial C_{g,j}}{\partial r} = 0$.
- ii. Tube inlet: the inlet concentrations in the gas phase were defined based on a small ozone and oxygen percentage by volume, $C_{g,j} = C_{g,j,0}$.
- iii. Tube outlet: the gas flux is predominantly by convection i.e., when $z = L$, $\frac{\partial C_{g,j}}{\partial z} = 0$.

2. Membrane section $R_i \leq r \leq (R_i + L_m)$

Momentum transport:

The velocity of gas in the membrane is assumed to be negligible, i.e., $\mathbf{u}_g = 0$. This is reasonable because of the low permeability of the gases in the membranes.

Species transport:

The steady state material balance for the transport of O_2 and O_3 across the membrane skin layer for the non-wetting mode of operation is considered to be due to diffusion only with no reactions taking place. The concentration profile can be described as follows:

$$D_{m,j} \left[\frac{1}{r} \frac{\partial}{\partial r} \left(r \frac{\partial C_{m,j}}{\partial r} \right) + \frac{\partial^2 C_{m,j}}{\partial z^2} \right] = 0 \quad (14)$$

where $C_{m,j}$ is the concentration of j in the membrane, $D_{m,j}$ is the mass diffusivity of j in the membrane and is assumed to be isotropic. Note that mass transport of mixed gases such as O_2/O_3 mixtures through membranes can be affected by coupling or competition effects of the involved gases [43]. For this study data for pure oxygen and ozone were used only without considering mutual interaction of gases within the membrane.

The boundary conditions were:

- i. Gas–membrane interface: the gas concentration is specified using the point-wise constraint boundary condition. The interfacial transport was defined by the solubility laws [26], i.e., when $r = R_i$, $C_{m1,j} = \frac{C_{g,j,i}}{S_j}$, where S_j is the solubility of j in the membrane.
- ii. Membrane inlet and outlet: the two boundaries are insulated, i.e., $\frac{\partial C_{m,j}}{\partial z} = 0$ at, $z = 0$ and $z = L$.

3. Liquid section $(R_i + L_m) \leq r \leq (R_i + L_m + L_w)$

Momentum transport:

The liquid is assumed to flow in the co-current configuration and is assumed to be steady, laminar and fully developed; hence the velocity can be described using the continuity and Navier–Stokes equations, as follows:

$$\text{Continuity : } \nabla \cdot \mathbf{u}_L \quad (15)$$

$$\text{Navier–Stokes : } \rho_L (\mathbf{u}_L \cdot \nabla \mathbf{u}_L) = -\nabla p_L + \mu_L \nabla^2 \mathbf{u}_L \quad (16)$$

where \mathbf{u}_L is the velocity vector in the liquid phase, and p_L is the pressure. The density and viscosity of the liquid are assumed constant throughout as ρ_L and μ_L , respectively.

The boundary conditions were:

- i. The velocity in the r -directions at all the boundaries are almost zero, i.e., $u_{r,L} = 0$
- ii. Membrane wall: no-slip, i.e., when $r = R_i + L_m$, $u_{z,L} = 0$.
- iii. Inlet: average velocity is specified at the inlet, i.e., when $z = 0$, $u_{z,L} = u_{L,mean}$.
- iv. Outlet: flow is fully developed, i.e., when $z = L$, $\frac{\partial u_{z,L}}{\partial z} = 0$.

Species transport:

The steady state material balance for the transport of O_2 and O_3 in the liquid phase may be written as follows:

$$\mathbf{u}_L \cdot \nabla C_{L,j} = D_{L,j} \nabla^2 C_{L,j} \quad (17)$$

where $C_{L,j}$ is the concentration of i in the liquid phase, $D_{L,j}$ is the mass diffusivity of i in the liquid phase and is assumed to be isotropic.

The boundary conditions were:

- i. Inlet: concentrations of O_2 and O_3 at the liquid inlet are assumed zero, i.e., $C_{L,j,0} = 0$.
- ii. Membrane–liquid interface: the gas concentration is specified using the point-wise constraint boundary condition. The interfacial transport was defined by the solubility laws [13], i.e., when $r = (R_i + L_m)$, $C_{m1,j} = H_j C_{L,j,i}$, where H_j is the Henry's constant of j in the liquid.

2.4. Mass Transfer Correlation

Empirical correlations for heat transfer can be used to describe local mass transfer resistances [13]. The mass transfer correlation was determined by the general form of the Sherwood number:

$$Sh = \frac{K_L L_c}{D} = A \cdot Re^B \cdot Sc^C \quad (18)$$

$$Re = \frac{\rho_L u_{L,mean} L_c}{\mu_L} \quad (19)$$

$$Sc = \frac{\mu_L}{D} \quad (20)$$

where L_c is the characteristic length taken as the hydraulic diameter of the liquid phase, i.e., $2L_w$, Re is the Reynolds number, Sc is the Schmidt number. A , B , and C are empirical constants and the value of C was assumed to be 0.33 [13,44].

3. Results and Discussion

The analysis of the membrane assisted mass transfer of ozone–oxygen gas mixtures into water consisted of determining the concentration profiles, mass transfer resistances in the gas, membrane, and liquid phases, and quantifying overall mass transfer coefficient with varying parameters such as membrane length, membrane thickness and liquid side velocities. Finally, a mass transfer correlation

based on a heat transfer analogy was proposed. The analysis was conducted both by including and excluding the effect of gas solubility within the membrane, termed ‘with S ’ and ‘without S ’ in this article respectively.

3.1. Concentration Profiles

The steady state radial concentration profiles of ozone and oxygen evaluated without S along the membrane at the inlet, 10% length, 50% length, and outlet are shown in Figure 4. The calculated concentration profiles for both gases match well with the expected profiles based on film theory (Figure 1). The profiles are generated by assuming continuous concentration at the gas–membrane interface, i.e., the solubility parameter S in Equation (2) equals 1. The concentration profile of ozone and oxygen in the gas phase is flat indicating the mass transfer resistance in the bulk gas is negligible. The bulk gas concentration decreases slightly with distance through the tube, as the ozone and oxygen both diffuse into the membrane and subsequently into the liquid phase. At the tube inlet, there is a sharp concentration gradient within the membrane indicating that the gases diffuse rapidly through the membrane, however, there is no instant ozone or oxygen transfer into the aqueous phase due to the resistance caused by the liquid film. The maximum concentration of O_3 and O_2 attainable at the outlet of the liquid phase are approximately 0.81 mol m^{-3} and 1.07 mol m^{-3} , respectively, along the length of the membrane. The profiles of ozone and oxygen appear similar because the diffusivities of both gases in each of the three phases are on the same order of magnitude (Table 1). The most contrasting difference is caused by the approximately 8-fold lower solubility of O_2 in water that leads to a large concentration drop at the membrane–liquid interface. Ozone decay and chemical reactions at the liquid side are not considered.

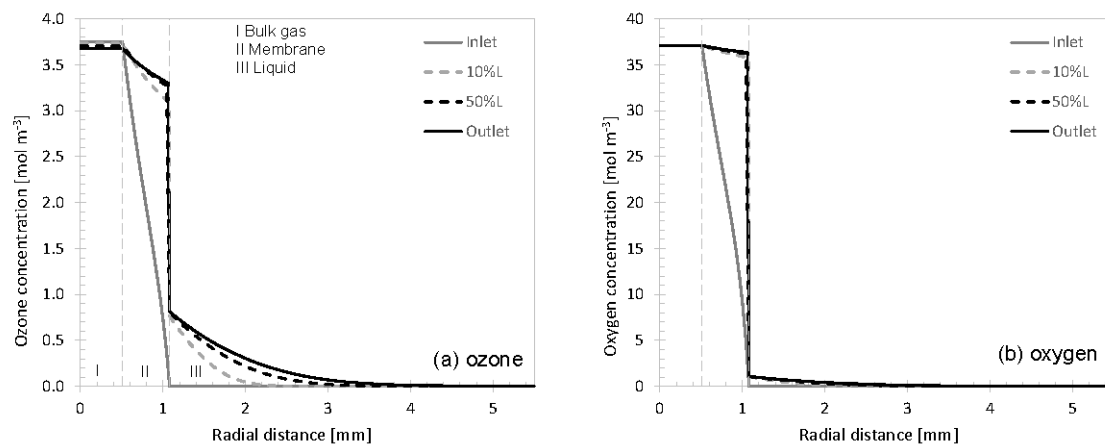


Figure 4. Concentration profiles evaluated without S at four different locations along the length of the tube, $L = 0.5 \text{ m}$ (inlet, 10% and 50% of length and outlet) for (a) ozone and (b) oxygen. The vertical dashed lines indicate the gas–membrane and membrane–liquid interfaces at $r = 0.51 \text{ mm}$ and $r = 1.08 \text{ mm}$, respectively. Conditions: $u_{g,\text{mean}} = 0.101 \text{ m s}^{-1}$, $u_{L,\text{mean}} = 0.008 \text{ m s}^{-1}$, $C_{g,o_3,0} = 3.75 \text{ mol m}^{-3}$, $C_{g,o_2,0} = 37.12 \text{ mol m}^{-3}$. Note the different concentration scales for ozone and oxygen.

Figure 5 shows the concentration profiles of the gases when the solubility of the gases in the membranes (S_{O_3} and S_{O_2} , Table 1) were taken into consideration. The marked difference in the profiles at the gas–membrane interface is caused and determined by the selectivity of the PDMS membrane. Including solubility in the modelling would represent more realistic concentration profiles. The solubility term adds an additional mass transfer resistance as indicated by the drop in concentration at the gas–membrane interface. In particular, the concentration of O_2 decreased significantly due to the much lower solubility of O_2 in PDMS compared to O_3 . This leads to a considerable decline in oxygen transfer into the liquid phase. For example, the maximum attainable concentration of O_2 at the outlet

of the liquid phase is approximately 0.22 mol/m^3 and thus 80% lower compared to the model without solubility, while O_3 concentration is 0.72 mol/m^3 and thus only 11% lower. Selectivity of membrane materials such as PDMS towards ozone mass transfer has important implications when considering off-gas recycling applications. For efficient use of O_3 , the membrane contacting area can be adjusted to provide selective depletion of O_3 at the gas side. Membrane material with O_3/O_2 separating properties, i.e., exhibiting high solubility ($S \rightarrow 1$) for O_3 and low solubility for O_2 ($S \rightarrow 0$) is desirable. The higher solubility of O_3 in PDMS has been ascribed to the higher boiling point and critical temperature of O_3 compared to O_2 that facilitates condensation into the polymer. It has also been argued that O_3 may initiate formation of peroxide groups at the membrane surface, which selectively increases O_3 solubility within PDMS [31].

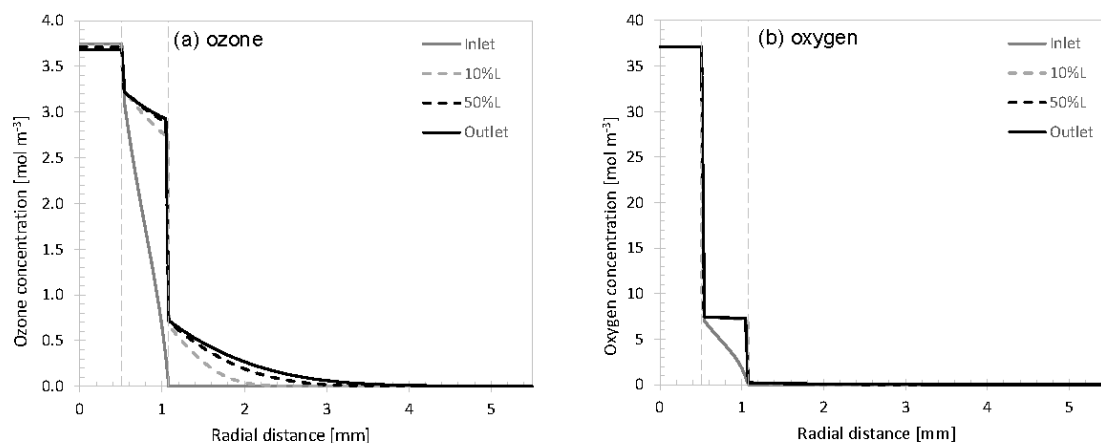


Figure 5. Concentration profiles evaluated with S at four differing locations along the length of the tube, $L = 0.5 \text{ m}$ (inlet, 10% and 50% of length and outlet) for (a) ozone and (b) oxygen. The vertical dashed lines indicate the gas–membrane and membrane–liquid interfaces at $r = 0.51 \text{ mm}$ and $r = 1.08 \text{ mm}$, respectively. Conditions: $u_{g,\text{mean}} = 0.101 \text{ m s}^{-1}$, $u_{L,\text{mean}} = 0.008 \text{ m s}^{-1}$, $C_{g,\text{O}_3,0} = 3.75 \text{ mol m}^{-3}$, $C_{g,\text{O}_2,0} = 37.12 \text{ mol m}^{-3}$, $S_{\text{O}_3} = 0.881$, $S_{\text{O}_2} = 0.201$.

Gas film, membrane, and liquid film mass transfer coefficients along the membrane were determined by using Equations (1), (4) and (5), respectively. To provide a more quantitative overview on the contribution of each coefficient than shown in the profile plots, the percentage mass transfer resistances (i.e., normalised reciprocal mass transfer coefficients) at 10% and 50% membrane length are shown in Figure 6. As indicated by the radial concentration profiles in Figures 4 and 5, the gas film resistances are negligible, contributing at most 0.01% towards the overall resistance. For the PDMS membrane and under the chosen liquid side flow conditions the most dominant resistance for O_2 mass transfer, with S and without S , resides within the membrane. This highlights the selectivity of the PDMS membranes. For O_3 , both the membrane resistance and the liquid film side resistance are important. In summary, this means that O_2 mass transfer can be controlled by selecting the appropriate membrane material, while O_3 mass transfer can also be adjusted by changes in liquid side parameters such as fluid velocity. For both gases, the solubility parameter, S , has relatively minor influence on the distribution of the individual mass transfer resistances. Nevertheless, solubility significantly affects the overall mass transfer coefficient, K_L , for both ozone and oxygen, as discussed in the following sections.

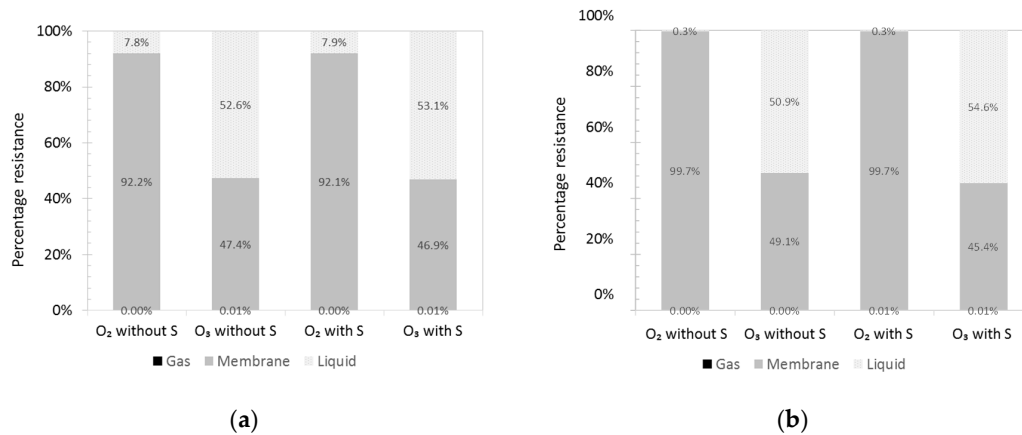


Figure 6. Percentage mass transfer resistances for oxygen and ozone with and without the solubility parameter for a tube of $L = 0.5$ m shown at (a) 10% tube length ($L = 50$ mm) and (b) 50% tube length ($L = 250$ mm). Conditions: $u_{g,mean} = 0.101$ m s⁻¹, $u_{L,mean} = 0.008$ m s⁻¹, gas–membrane and membrane–liquid interfaces are located at $r = 0.51$ mm and $r = 1.08$ mm, respectively, $S_{O_3} = 0.881$, $S_{O_2} = 0.201$.

3.2. Variation of Model Parameters

The overall mass transfer coefficients, K_L , for ozone and oxygen were calculated using Equation (10). The effects of membrane tube length, thickness of membrane, liquid side velocity, and inlet gas concentration on the overall mass transfer were determined, while other model parameters were kept unchanged. Results with and without considering membrane solubility are presented.

3.2.1. Tube Length

The effect of tube length on the average overall mass transfer coefficient is shown in Figure 7. Lengths between 250 and 1500 mm were considered reasonable for a typical membrane module. According to the inverse relationship between tube length and K_L (Equation (10)), the overall mass transfer coefficient decreases with increasing length, e.g., by 1/3 when doubling the length of the membrane. Figure 7a shows that the difference in the overall mass transfer coefficient for O₃ between the case with and without solubility is relatively small, i.e., approximately 30%. On the other hand, in Figure 7b, the difference in O₂ is more than one order of magnitude. This again highlights the importance of the solubility parameter in the analysis of ozone or oxygen transfer through non-porous membranes.

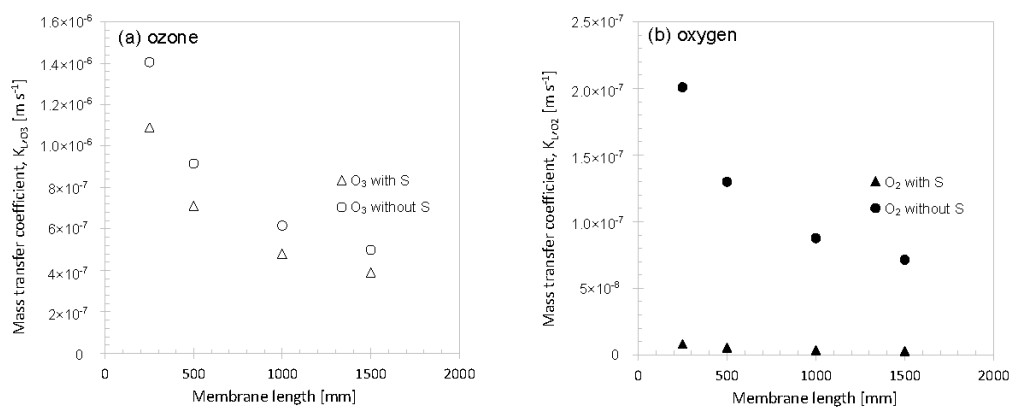


Figure 7. Effect of membrane tube length on the overall mass transfer coefficient K_L for (a) ozone and (b) oxygen. Conditions: $u_{g,mean} = 0.101$ m s⁻¹, $u_{L,mean} = 0.008$ m s⁻¹, gas–membrane and membrane–liquid interfaces are located at $r = 0.51$ mm and $r = 1.08$ mm, respectively, $S_{O_3} = 0.881$, $S_{O_2} = 0.201$.

3.2.2. Membrane Thickness

The effect of membrane thickness on the overall mass transfer coefficient is shown in Figure 8. Membrane thickness was varied by examining the outer tube radii from 0.01 mm to 6.0 mm, while keeping the inner tube radius constant. Very thin membranes are not realistic under actual application conditions, unless used as coatings or an internal layer and stabilised by supporting materials. At small membrane thicknesses, typically <1.0 mm, the overall mass transfer coefficient decreases rapidly by adding a membrane layer as an additional mass transfer resistance, in particular for O₂, for which the membrane is the dominating resistance. It is interesting to see that for O₃, there is an initial increase in mass transfer, which indicates the presence of a critical radius at 0.25 mm. This is analogous to the critical radius observed in heat insulation of a tube. This observation, however, requires further computational and experimental validation work. Apart from this unusual effect at a small membrane thickness, increasing the membrane thickness decreases the overall mass transfer coefficient. To minimise the mass transfer resistance, it is recommended that membranes are selected that are as thin as possible while still considering factors like mechanical strength, fouling resistance, lifetime performance, and costs [13]. Overall, the membrane thickness has a more significant effect on the mass transfer than the liquid length, but is less influential than the tube side velocity discussed in the next section.

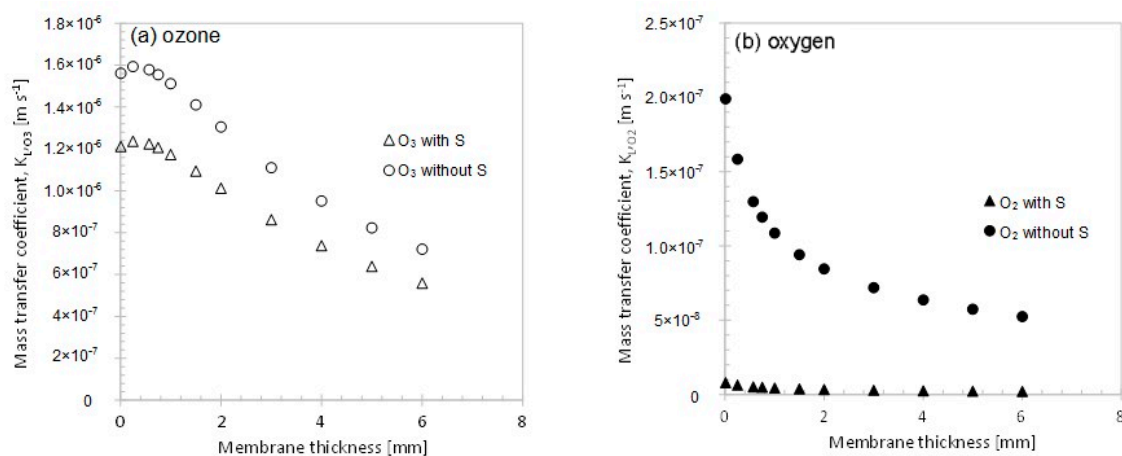


Figure 8. Effect of membrane thickness on the overall mass transfer coefficient K_L for (a) ozone and (b) oxygen. Conditions: $u_{g,mean} = 0.101 m s^{-1}$, $u_{L,mean} = 0.008 m s^{-1}$, $S_{O_3} = 0.881$, $S_{O_2} = 0.201$, tube length $L = 0.5 m$, the gas–membrane interface is located at $r = 0.51$ at (location). The outer membrane tube radius is the sum of the inner tube radius and the membrane thickness.

3.2.3. Liquid Side Velocity

The liquid side velocity $u_{L,mean}$ was varied from $0.4 mm s^{-1}$ to $250 mm s^{-1}$ corresponding to the liquid side Reynolds number, Re , of 3.5 to 2210, respectively. Figure 9 shows that the mass transfer coefficient strongly increases with increasing liquid side velocity, at a factor of approximately 57 and 37 within the considered velocity range for oxygen and ozone, respectively. At a velocity of $250 mm s^{-1}$, which corresponds to a Re of 2210, the increasing effect of liquid side velocity on mass transfer starts to level off. This is in agreement with a previous study that found that ozone mass transfer becomes independent of Re above a value of around 2000 [13]. The data points at the highest velocity that do not fit in the power law trend line suggest a flow close to the transitional flow regime. Modelling in the transitional and turbulent flow regime is currently in progress.

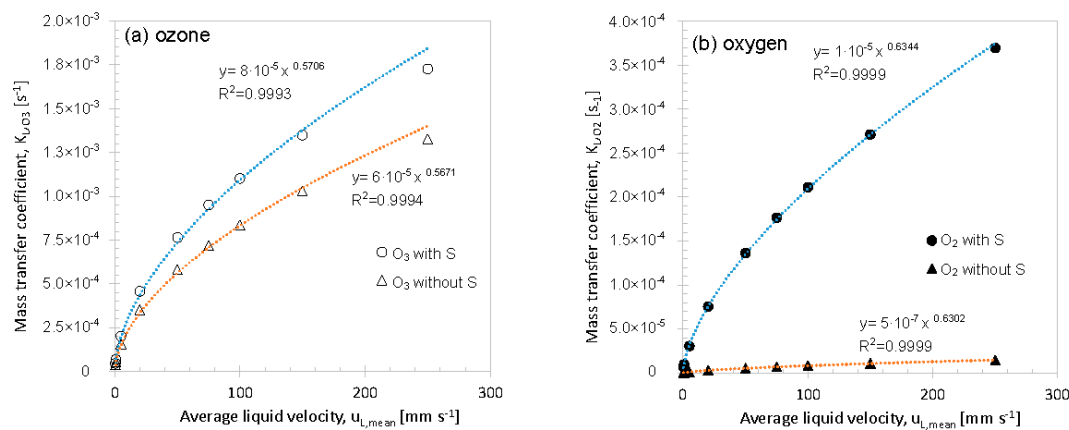


Figure 9. Effect of liquid side velocity on the overall mass transfer coefficient K_L for (a) ozone and (b) oxygen. Conditions $u_{g,mean} = 0.101 \text{ m s}^{-1}$, tube length $L = 0.5 \text{ m}$, gas–membrane and membrane–liquid interfaces are located at $r = 0.51 \text{ mm}$ and $r = 1.08 \text{ mm}$, respectively, $S_{O_3} = 0.881$, $S_{O_2} = 0.201$.

The effect of inlet gas concentration of ozone ranging from 0.41 to 6.25 mol m^{-3} on the overall mass transfer coefficient was also explored (data not shown). It was found that the inlet gas concentration had a negligible influence on the calculated K_L values, which implied that the mass transfer coefficient was mostly independent of the inlet gas concentration produced by commercially available ozone generators.

Among the variations investigated, changes in the liquid side velocity had the most significant effect on the overall mass transfer coefficient for ozone. This is in agreement with previous studies [13,36], and confirmed that ozone mass transfer is controlled by the liquid phase. Membrane thickness also had a significant influence on K_L , while tube length only had a small effect and mass transfer was seemingly independent of the inlet ozone gas concentration.

3.3. Mass Transfer Correlation

Using the heat transfer analogies outlined in Section 2.4 (Equations (18)–(20)), the mass transfer relationships between Sh , Re , and Sc were formulated for PDMS membranes. The relationships of Re and Sc are similar to plots for the overall mass transfer coefficients versus average liquid velocity shown in Figure 9, and therefore are not shown here. The relationships for O_2 and O_3 based on the model with and without solubility are summarised alongside with correlations from literature in Table 3. Comparison with semi-empirical correlations for a non-porous Teflon membrane and a general relationship based on the film model show good agreement in the Re exponent, indicating that the computational approach used in this study provides reasonable results to quantify ozone and oxygen mass transfer through membranes. The dependence of Sh on the Re is similar for both models which confirms that the solubility of the gases in the membrane is independent of flow conditions.

Table 3. Gas mass transfer correlations for non-porous membrane contactor systems and general equation based on film model derived from heat and mass transfer analogy.

Membrane System	Correlation	Reference
PDMS, non-porous, without solubility (S)	$Sh_{O_2} = 8.66Re_L^{0.634}Sc_{O_2}^{0.33}$ $Sh_{O_3} = 100Re_L^{0.571}Sc_{O_3}^{0.33}$	This study
PDMS, non-porous, with solubility (S)	$Sh_{O_2} = 0.353Re_L^{0.63}Sc_{O_2}^{0.33}$ $Sh_{O_3} = 78.1Re_L^{0.567}Sc_{O_3}^{0.33}$	This study
Teflon, non-porous, without solubility (S)	$Sh = 0.136Re_L^{0.73}Sc_{O_3}^{0.33}$	[13]
Film model [Heat and mass transfer analogy]	$Sh = 0.332Re^{0.5}Sc_{O_3}^{0.33}$	[45]

4. Conclusions

The mass transfer of ozone and oxygen into the aqueous phase through a single tubular non-porous polymeric membrane was studied using CFD modelling and applying fundamental convection-diffusion theory. A computational approach to visualise concentration profiles across the membrane and at the gas–membrane–liquid interfaces was developed. Single mass-transfer resistances were quantified and a parameter variation study was conducted. The results are in accordance with qualitative predictions made by traditional film theory and generally align with results of prior experimental studies on the mass transfer of ozone via membranes for water treatment applications [13,19,31]. The introduction of previously unstudied solubility effects for oxygen and ozone in polymeric membranes into the model resulted in more accurate mass transfer predictions for both gases. It was shown that the solubility effect for oxygen is particularly important for the studied PDMS polymer and selective ozone transfer may be achieved. To further consolidate the presented model, it will be important to consider mutual effects of ozone and oxygen for their transport through non-porous membranes in future studies [46], which also includes experimental approaches to quantify these effects.

Ozone membrane contacting can be regarded as an alternative for conventional ozone contacting in areas of application where oxygen recycling is economically interesting and in space restricted locations. Bubble-less ozonation, including high mass transfer even under low-flow laminar conditions, can be advantageous for smaller volumes or intermediate water treatment steps in combination with sand filtration or soil passages. Furthermore, a membrane facilitated O_3/H_2O_2 (peroxone) process was developed to mitigate the formation of bromate [47], a potentially carcinogenic ozonation byproduct. Understanding transfer processes in small membrane sections such as single tubes is important to provide a basis for reactor design and developing more sophisticated models that include chemical reactions of ozone at the liquid side and more complicated flow conditions occurring, for example in cross-flow shell-and tube designs with internal water flow.

Acknowledgments: Financial support for undergraduate research projects of M.J.B. and W.K. by the Department of Chemical Engineering and start-up infrastructure funding by the Faculty of Engineering & Design for J.W. is appreciated. C.M.T. was supported by an EPSRC funded integrated Ph.D. studentship in Sustainable Chemical Technologies. The authors thank Urs von Gunten for valuable comments on the manuscript and Charlotte Wilkes for proof reading.

Author Contributions: Y.M.J.C. and J.W. designed the modelling part of the study; M.J.B. and W.K. performed the computational fluid dynamics modelling and interpreted the results; C.M.T.; M.J.B. and J.W. conducted the literature research; Y.M.J.C. and J.W. wrote the paper.

Conflicts of Interest: The authors declare no conflict of interest.

Abbreviations

Nomenclature

<i>a</i>	Interfacial surface area of membrane per unit volume of liquid	$m^2 m^{-3}$
<i>C</i>	Concentration	$mol m^{-3}$
<i>D</i>	Diffusivity	$m^2 s^{-1}$
<i>H</i>	Henry's Law constant	-
<i>k</i>	Mass transfer coefficient	$m s^{-1}$
<i>K_L</i>	Overall mass transfer coefficient	$m s^{-1}$
<i>L</i>	Length	m
<i>N</i>	Molar flux	$mol m^{-2} s^{-1}$
<i>p</i>	Pressure	Pa
<i>r</i>	Radial coordinate	m

Nomenclature

R	Mass transfer resistance	m s^{-1}
R	Radius	m
R_i	Inner membrane radius	m
R_g	Universal gas constant	$\text{J mol}^{-1} \text{K}^{-1}$
Re	Reynold's Number	-
S	Solubility coefficient	-
$S_{i,03}$	Solubility of ozone in PDMS = 3.55×10^{-1} [26]	$\text{mol m}^{-3} \text{Pa}^{-1}$
Sc	Schmidt Number	-
Sh	Sherwood Number	-
T	Temperature	K
$Q_{m,03}$	Permeability coefficient of ozone in PDMS = 1.05×10^{-9} [31]	$(\text{mol m}) \text{m}^{-2} \text{s}^{-1} \text{Pa}^{-1}$
\mathbf{u}	Velocity vector	m s^{-1}
u	Velocity	m s^{-1}
z	Axial coordinate	m
μ	Viscosity	Pa s
ρ	Density	kg m^{-3}

Subscripts

c	Characteristic
g	Gas phase
i	Interface
$inner$	Inner
j	Component j
L	Liquid phase
m	Membrane
$mean$	Mean or average value
0	Inlet
O_2	Oxygen
O_3	Ozone
$outer$	Outer
Out	Outlet
tot	Total
w	Characteristic length scale of water phase

Acronyms

CFD	Computational fluid dynamics
PDMS	Polydimethylsiloxane
PTFE	Polytetrafluoroethylene
PVDF	Polyvinylidene difluoride

References

- Loeb, B.L.; Thompson, C.M.; Drago, J.; Takahara, H.; Baig, S. Worldwide ozone capacity for treatment of drinking water and wastewater: A review. *Ozone Sci. Eng.* **2012**, *34*, 64–77. [[CrossRef](#)]
- Gottschalk, C.; Libra, J.A.; Saupe, A. *Ozonation of Water and Waste Water a Practical Guide to Understanding Ozone and Its Applications*, 2nd ed.; Wiley: Weinheim, Germany, 2010; p. 362.
- Rakness, K.L. *Ozone in Drinking Water Treatment: Process Design, Operation, and Optimization*; American Water Works Association: Denver, CO, USA, 2011; p. 305.
- Dodd, M.C.; Zuleeg, S.; von Gunten, U.; Pronk, W. Ozonation of source-separated urine for resource recovery and waste minimization: Process modeling, reaction chemistry, and operational considerations. *Environ. Sci. Technol.* **2008**, *42*, 9329–9337. [[CrossRef](#)] [[PubMed](#)]
- Zhou, H.; Smith, D.W.; Stanley, S.J. Modeling of dissolved ozone concentration profiles in bubble columns. *J. Environ. Eng.* **1994**, *120*, 821–840. [[CrossRef](#)]
- Zhou, H.; Smith, D.W. Ozone mass transfer in water and wastewater treatment: Experimental observations using a 2d laser particle dynamics analyzer. *Water Res.* **2000**, *34*, 909–921. [[CrossRef](#)]

7. Hollender, J.; Zimmermann, S.G.; Koepke, S.; Krauss, M.; McArdell, C.S.; Ort, C.; Singer, H.; von Gunten, U.; Siegrist, H. Elimination of organic micropollutants in a municipal wastewater treatment plant upgraded with a full-scale post-ozonation followed by sand filtration. *Environ. Sci. Technol.* **2009**, *43*, 7862–7869. [[CrossRef](#)] [[PubMed](#)]
8. Langlais, B.; Reckhow, D.A.; Brink, D.R. *Ozone in Water Treatment: Application and Engineering: Cooperative Research Report*; CRC Press (Lewis Publishers): Boca Raton, FL, USA, 1991.
9. Battimelli, A.; Millet, C.; Delgenès, J.P.; Moletta, R. Anaerobic digestion of waste activated sludge combined with ozone post-treatment and recycling. *Water Sci. Technol.* **2003**, *48*, 61–68. [[PubMed](#)]
10. Oneby, M.A.; Bromley, C.O.; Borchardt, J.H.; Harrison, D.S. Ozone treatment of secondary effluent at U.S. Municipal wastewater treatment plants. *Ozone Sci. Eng.* **2010**, *32*, 43–55. [[CrossRef](#)]
11. Kerry, F.G. *Industrial Gas Handbook: Gas Separation and Purification*; CRC Press: Boca Raton, FL, USA, 2007; p. 550.
12. Gabelman, A.; Hwang, S.T. Hollow fiber membrane contactors. *J. Membr. Sci.* **1999**, *159*, 61–106. [[CrossRef](#)]
13. Pines, D.S.; Min, K.N.; Ergas, S.J.; Reckhow, D.A. Investigation of an ozone membrane contactor system. *Ozone Sci. Eng.* **2005**, *27*, 209–217. [[CrossRef](#)]
14. Drioli, E.; Criscuoli, A.; Curcio, E. Membrane contactors fundamentals, applications and potentialities. In *Membrane Science and Technology Series 11*; Elsevier: Amsterdam, The Netherlands, 2006; p. 516.
15. Li, N.N.; Fane, A.G.; Ho, W.S.W.; Matsuura, T. *Advanced Membrane Technology and Applications*; Wiley-Blackwell: Oxford, UK, 2008; p. 994.
16. Ismail, A.F.; Khulbe, C.; Matsuura, T. *Gas Separation Membranes*; Springer: Berlin, Germany, 2015; p. 331.
17. Mulder, M. *Basic Principles of Membrane Technology*, 2nd ed.; Kluwer: Dordrecht, The Netherlands; London, UK, 1996; p. 564.
18. Shen, Z.; Semmens, M.J.; Collins, A.G. A novel approach to ozone—Water mass transfer using hollow—Fiber reactors. *Environ. Technol.* **1990**, *11*, 597–608. [[CrossRef](#)]
19. Dos Santos, F.R.A.; Borges, C.P.; da Fonseca, F.V. Polymeric materials for membrane contactor devices applied to water treatment by ozonation. *Mater. Res.* **2015**, *18*, 1015–1022. [[CrossRef](#)]
20. Janknecht, P.; Wilderer, P.A.; Picard, C.; Larbot, A. Ozone-water contacting by ceramic membranes. *Sep. Purif. Technol.* **2001**, *25*, 341–346. [[CrossRef](#)]
21. Picard, C.; Larbot, A.; Sarrazin, J.; Janknecht, P.; Wilderer, P. Ceramic membranes for ozonation in wastewater treatment. *Ann. Chim. Sci. Mater.* **2001**, *26*, 13–22. [[CrossRef](#)]
22. Stylianou, S.K.; Szymanska, K.; Katsoyiannis, I.A.; Zouboulis, A.I. Novel water treatment processes based on hybrid membrane-ozonation systems: A novel ceramic membrane contactor for bubbleless ozonation of emerging micropollutants. *J. Chem.* **2015**, *1–12*, 214927. [[CrossRef](#)]
23. Stylianou, S.K.; Kostoglou, M.; Zouboulis, A.I. Ozone mass transfer studies in a hydrophobized ceramic membrane contactor: Experiments and analysis. *Ind. Eng. Chem. Res.* **2016**, *55*, 7587–7597. [[CrossRef](#)]
24. Heng, S.; Yeung, K.L.; Djafer, M.; Schrotter, J.C. A novel membrane reactor for ozone water treatment. *J. Membr. Sci.* **2007**, *289*, 67–75. [[CrossRef](#)]
25. Atchariyawut, S.; Phattaranawik, J.; Leiknes, T.; Jiratananon, R. Application of ozonation membrane contacting system for dye wastewater treatment. *Sep. Purif. Technol.* **2009**, *66*, 153–158. [[CrossRef](#)]
26. Dingemans, M.; Dewulf, J.; van Hecke, W.; van Langenhove, H. Determination of ozone solubility in polymeric materials. *Chem. Eng. J.* **2008**, *138*, 172–178. [[CrossRef](#)]
27. Leiknes, T.; Phattaranawik, J.; Boller, M.; von Gunten, U.; Pronk, W. Ozone transfer and design concepts for nom decolourization in tubular membrane contactor. *Chem. Eng. J.* **2005**, *111*, 53–61. [[CrossRef](#)]
28. Bamperng, S.; Suwannachart, T.; Atchariyawut, S.; Jiratananon, R. Ozonation of dye wastewater by membrane contactor using PVDF and PTFE membranes. *Sep. Purif. Technol.* **2010**, *72*, 186–193. [[CrossRef](#)]
29. Jansen, R.H.S.; de Rijk, J.W.; Zwijnenburg, A.; Mulder, M.H.V.; Wessling, M. Hollow fiber membrane contactors—A means to study the reaction kinetics of humic substance ozonation. *J. Membr. Sci.* **2005**, *257*, 48–59. [[CrossRef](#)]
30. Shanbhag, P.V.; Guha, A.K.; Sirkar, K.K. Membrane-based ozonation of organic compounds. *Ind. Eng. Chem. Res.* **1998**, *37*, 4388–4398. [[CrossRef](#)]
31. Shanbhag, P.V.; Sirkar, K.K. Ozone and oxygen permeation behavior of silicone capillary membranes employed in membrane ozonators. *J. Appl. Polym. Sci.* **1998**, *69*, 1263–1273. [[CrossRef](#)]

32. Phattaranawik, J.; Leiknes, T.; Pronk, W. Mass transfer studies in flat-sheet membrane contactor with ozonation. *J. Membr. Sci.* **2005**, *247*, 153–167. [[CrossRef](#)]
33. Zhang, J.; Tejada-Martinez, A.E.; Lei, H.; Zhang, Q. Indicators for technological, environmental and economic sustainability of ozone contactors. *Water Res.* **2016**, *101*, 606–616. [[CrossRef](#)] [[PubMed](#)]
34. Cockx, A.; Do-Quang, Z.; Liné, A.; Roustan, M. Use of computational fluid dynamics for simulating hydrodynamics and mass transfer in industrial ozonation towers. *Chem. Eng. Sci.* **1999**, *54*, 5085–5090. [[CrossRef](#)]
35. Ghasem, N.; Al-Marzouqi, M.; Abdul Rahim, N. Modelling of CO₂ absorption in a membrane contactor considering solvent evaporation. *Sep. Purif. Technol.* **2013**, *110*, 1–10. [[CrossRef](#)]
36. Al-Saffar, H.B.; Ozturk, B.; Hughes, R. A comparison of porous and non-porous gas-liquid membrane contactors for gas separation. *Chem. Eng. Res. Des.* **1997**, *75*, 685–692. [[CrossRef](#)]
37. Mansourizadeh, A. Experimental study of CO₂ absorption/stripping via PVDF hollow fiber membrane contactor. *Chem. Eng. Res. Des.* **2012**, *90*, 555–562. [[CrossRef](#)]
38. Coulson, J.M.; Richardson, J.F. *Coulson & Richardson's Chemical Engineering: Fluid Flow, Heat Transfer, and Mass Transfer*, 6th ed.; Elsevier (Butterworth-Heinemann): Oxford, UK, 1999; p. 895.
39. Tu, J.; Yeoh, G.H.; Liu, C. *Computational Fluid Dynamics: A Practical Approach*; Elsevier (Butterworth-Heinemann): Oxford, UK, 2012; p. 456.
40. Massman, W.J. A review of the molecular diffusivities of H₂O, CO₂, CH₄, CO, O₃, SO₂, NH₃, N₂O, NO, and NO₂ in air, O₂ and N₂ near STP—Polar and polyatomic gases. *Atmos. Environ.* **1998**, *32*, 1111–1127. [[CrossRef](#)]
41. Tritton, D.J. *Physical Fluid Dynamics*; Springer: Dordrecht, The Netherlands, 2012; p. 362.
42. Sander, R. Compilation of Henry's law constants (version 4.0) for water as solvent. *Atmos. Chem. Phys.* **2015**, *15*, 4399–4981. [[CrossRef](#)]
43. Dhingra, S.S.; Marand, E. Mixed gas transport study through polymeric membranes. *J. Membr. Sci.* **1998**, *141*, 45–63. [[CrossRef](#)]
44. Bird, R.B.; Stewart, W.E.; Lightfoot, E.N. *Transport Phenomena*; John Wiley & Sons: Oxford, UK, 2007; p. 905.
45. Bergman, T.L.; Incropera, F.P.; de Witt, D.P.; Lavine, A.S. *Fundamentals of Heat and Mass Transfer*, 7th ed.; John Wiley & Sons: Oxford, UK, 2011.
46. Yampolskii, Y. Polymeric gas separation membranes. *Macromolecules* **2012**, *8*, 3298–3311. [[CrossRef](#)]
47. Merle, T.; Pronk, W.; von Gunten, U. MEMBRO3X, a novel combination of a membrane contactor with advanced oxidation (O₃/H₂O₂) for simultaneous micropollutant abatement and bromate minimization. *Environ. Sci. Technol. Lett.* **2017**, *4*, 180–185. [[CrossRef](#)]



© 2017 by the authors. Licensee MDPI, Basel, Switzerland. This article is an open access article distributed under the terms and conditions of the Creative Commons Attribution (CC BY) license (<http://creativecommons.org/licenses/by/4.0/>).